Thermal Enhanced Electrokinetic Bacterial Transport in Porous Media

Yongping Shan[1], Huijuan Hao[1], Jinyao He[2], Naiwen Hu[1], Ping Liu[1], Mingxiu Zhan[3], Wentao Jiao[1]*, and Yongguang Yin[1]

[1] *Research Center for Eco-Environmental Sciences, Chinese Academy of Sciences, 100085 Beijing, China.*

[2] *UFZ - Helmholtz Centre for Environmental Research, Department of Environmental Microbiology, 04318 Leipzig, Germany.*

[3] *College of Metrology and Measurement Engineering, China Jiliang University, Hangzhou 310018 Zhejiang, China.*

[*] Corresponding author: E-mail: wtjiao@rcees.ac.cn (W. Jiao).

Abstract: Soil bacterial communities are crucial to various ecosystem services, with significant implications for environmental processes and human health. Delivering functional bacterial strains to target locations enhances preferred ecological features. However, the delivery process is often constrained by limited bacterial transport through low-permeability soil. Although electrokinetics breaks the bottleneck of bacterial transport in thin porous media, its efficiency remains limited. Here, we tested the hypothesis that thermal effects enhance electrokinetic transport by shifting the net force acting on the bacterium. We found that heating significantly increased electrokinetic transport by 2.75-fold at 1 V cm^{-1} through porous media. Thermal enhancement mechanisms were interpreted by the heating shift of net force integrating matrix attractive and electrokinetic forces, and verified by the Quartz Crystal Microbalance with Dissipation Monitoring (*QCMD*) observed adhesion rigidity shift. Thermal-dependent parameters liquid viscosity and dielectric constant were the primary contributors to the net force shift. Their variations reduce the attractive force and augment the electrokinetic forces, resulting in lower adhesion rigidity and enhanced bacterial transport. A mechanism-based approach interlinking electric field strength, thermal effect, and collision efficiency was established to facilitate the application of thermally enhanced electrokinetic bacterial transport. These findings provide new prospects for improving bacterial transport, hence optimizing soil ecosystem functions.

Keywords: thermal enhancement; electrokinetics; bacterial transport; low-permeability soil

Synopsis: This study reports a significant enhancement of thermal effects on the electrokinetic bacterial transport in porous media.

46 **TOC Art**

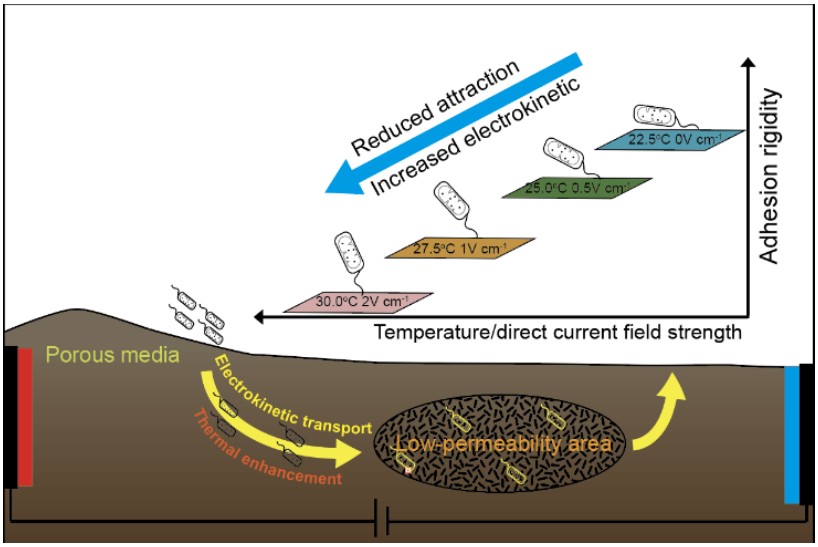
Reduced attraction
Increased electrokinetic
22.5°C 0V cm⁻¹
25.0°C 0.5V cm⁻¹
27.5°C 1V cm⁻¹
30.0°C 2V cm⁻¹
Adhesion rigidity
Temperature/direct current field strength
Porous media
Electrokinetic transport
Thermal enhancement
Low-permeability area

47

1. Introduction

Bacteria play essential roles in fulfilling soil ecosystem functions, e.g., soil priming,[1] nutrient amendment,[2] and environmental remediation.[3,4] They support a range of critical processes that sustain natural and engineered ecosystems.[5,6] Bioengineering approaches enable intervening bacterial communities by delivering functional bacterial strains to preferred sites, achieving target ecosystem services with consequences for environmental and human health[7]. However, the realization of bacterial activities in practical applications is often constrained during bacterial transport to target uptake spots in low-permeability porous media, especially through thin pore networks.[8,9] Therefore, approaches that enhance bacterial transport in porous media are crucial for the development of bioremediation technology[10].

Current strategies in improving bacterial transport include fluid shear, direct current (DC) field, etc.[11–14] DC field shows potential in facilitating bacterial transport through low-permeable soil structures, by introducing electrokinetic phenomena, such as electroosmosis and electrophoresis.[15,16] Contrary to the parabolic hydraulic fluid, the plug-shaped electroosmotic flow acts at several nanometers above matrix surfaces. It allows for mobilization in microscale channels that are typically not affected by hydraulic flow. It thus acts in the scales of low-permeable soil pore networks relevant for the microbe-matrix interactions and promotes bacterial transport[17]. Electrokinetics performs better in enhancing the transport of high surface charge hydrophilic bacterial strains compared to low surface charge hydrophobic ones.[18] Electrokinetic enhancement on a typical high surface charged bio-degrader of polycyclic aromatic hydrocarbons *Pseudomonas fluorescens* LP6a through porous media reaches 85% under a weak DC field of 3 V cm^{-1}.[19] However, in practical application, applying high voltage electric fields in a long-term cause unwanted variations in pH, redox potential, and soil structure. The electrokinetic transport rate still represents a significant hinderance of the bio-

degrader through long-distance delivery. Therefore, there is interest in further enhancing electrokinetic bacterial transport through porous media to reduce the required DC field strength.

Electrokinetic bacterial transport is driven by the interactions of the matrix attractive force, electroosmotic shear force, and electrophoretic drag force.[18] Thermal effects alter environmental physicochemical properties including liquid viscosity[20], dielectric constant[21], and zeta potentials of bacteria and solid surface[22]. Theoretically, the reduction of these physicochemical parameters has the potential to reduce matrix attractive force (cf. eq. S8) and increase electrokinetic velocities (cf. eqs. S13-S14)[23]. There is, hence interest in testing the hypothesis that thermal effects enhance electrokinetic bacterial transport by introducing variations in the physical environment.

Here, based on the principles of microbe-matrix interaction, electroosmosis, and electrophoresis, we hypothesize that heating promotes bacterial transport driven by the thermal-dependent net force acting on bacterial cells. Thermal enhancement of electrokinetic bacterial transport was investigated in percolation columns, and evidenced by the high-sensitivity measurement of the bacteria-quartz adhesion rigidity in the quartz crystal microbalance with dissipation (*QCMD*) system. Thermal effects on electrokinetic bacterial transport were evaluated using clean-bed filtration theory[24]. The mechanisms were interpreted by the shift of net force integrating matrix attractive and electrokinetic forces, and verified by the *QCMD* observed adhesion rigidity shift. The thermal-dependent parameters driving net force shift including the liquid viscosity, dielectric constant, and zeta potentials were derived from the equations, and their impact extent was investigated. The findings may support better prediction of thermal electrokinetic improvement on bacterial transport, hence optimizing soil ecosystem functions.

2. Materials and Methods

2.1 Cultivation of Bacteria and Inoculum Preparation

Pseudomonas fluorescens LP6a (GenBank accession No. AF525494)[25] was selected as the model electrokinetic transport strain, adopted following our previous research. It was cultivated in lysogeny broth (LB) medium until the early stationary phase (18 h at 25 °C, 150 rpm). The cultures were then centrifuged (5000 ×*g*, 10 min), and resuspended (SCI-FS, Scilogex, China) in 100 mM potassium phosphate buffer (PB, pH = 7.0, prepared with 61 mmol K_2HPO_4 and 39 mmol KH_2PO_4 diluted in 1 L DI water). The centrifuge-vortex treatment was repeated three times to reduce extracellular polymeric substances. Afterward, cell suspension in PB was diluted to an optical density of 0.30 at 600 nm using a UV/vis spectrophotometer (Evolution 160, Thermo Fisher Scientific, Carlsbad, CA). In practical applications, the optical density of 0.30 enables the colonization of bio-degraders in the soil, while avoiding unnecessary dynamic coagulation of over-density.

2.2 Characterization of Physiochemical Properties

The zeta-potentials of bacteria (ζ_{bac}), sand (ζ_s), and the silica sensor of quartz crystal microbalance (*QCMD*) (ζ_{sr}) were measured by Doppler electrophoretic light scattering analysis (Zetasizer Nano ZS90, Malvern, UK) with disposal folded capillary cells. The sand particles were sampled from a riverside, sieved to 1mm diameter, washed with DI water, dried in oven, and stored in a desiccator before usage. The zeta potential of sand particles was estimated using smashed sand sieved to diameter < 100 μm, treated at 200°C in a muffle furnace for 2 h, then cooled to room temperature (25°C) under sterile conditions. The contact angles (θ) of *P.* LP6a and sand were measured using a drop-shape analysis system (DSA100, KRÜSS, Germany) in three solvents water, formamide, and methylene iodide[19,26] and listed in Table S1. Bacterial lawns for drop-shape analysis were prepared by depositing bacteria from inoculated suspensions on cellulose acetate membrane filters (Millipore, 0.45 μm). Sand lawns for drop-shape analysis were prepared following the protocol of Achtenhagen et al.[27] Three sand lawns

were prepared for each experiment, with three solvent droplets of the drop-shape analysis system applied per lawn. The contact angles of solvents at the moment of dropping on the lawns were captured by a high-speed camera.

2.3 Thermal Electrokinetic Transport Experiments

Electrokinetic column experiments Electrokinetic percolation columns adapted from previous work[28] were immersed in a temperature-conditioning water bath (DLSB 5L/10, Yuhua, China) to conduct bacterial transport experiments (Fig. S1). The columns were sterilized and wet-packed with clean, sterilized sand in PB, achieving a porosity of 0.30 and a pore volume (PV) of 3.99 mL. The water bath maintained static temperature of the bacterial suspension reservoir and columns at 20, 30, 40, and 50˚C, with deviations ≤ 2°C.

Prior to the experiments, the columns were equilibrated for 30 min by circulating clean PB at the target temperature using a peristaltic pump (310HT, SENZ, China). The bacterial suspension with an optical density (OD) of 0.30 at 600 nm, was stirred and temperature-stabilized while pumping through the columns downward at an advective flow rate of 19.6 mL h^{-1} (equivalent to 2.4×10^{-7} m s^{-1} in the porous media). Bacterial transport was quantified by measuring the OD of both the influent (C_0) and effluent (C) at an interval of 5 min (equivalent to 0.41 PV) over a period of three hours.

After column experiments, the viability of bacterial suspension in the reservoir was assessed via flow cytometry (Novocyte 1040, ACEA, USA). Nucleic acid stain propidium iodide (PI, Thermofisher, USA) was used to label dead cells. Bacterial suspensions were centrifuged (3200 ×g, 10 min, 4°C), washed with 100 mmol L^{-1} phosphate buffer 3 times by centrifuge-vortex process, to exclude the effects of extracellular polymeric substances (EPS), and adjusted to a cell concentration magnitude of 10^6 cell mL^{-1}. Then 100 μL bacterial suspension was mixed with 5 μL of 100 μg mL^{-1} PI, incubated in the dark for 15 min, and analyzed by flow cytometry.

The flow cytometric settings were: fluorescence voltage 420 mV, forward scatter (FSC) threshold 1000, and the count rate 1000 cells s^{-1}.

QCMD experiments with flow cytometry quantification Time-resolved high-sensitivity Quartz Crystal Microbalance with Dissipation Monitoring (*QCMD*) allows analysis of cell adhesion behavior at the liquid-solid interface.[29,30] *QCMD* reflects the amount and viscoelastic properties of an adhering mass (bacteria) by changes in the resonance frequency (Δf) and changes in the energy dissipation (ΔD) of an oscillating crystal coating sensor surface[31]. *QCMD* (Q-Sense Explorer, Biolin Scientific, Sweden) experiments were conducted to assess the impact of heating and electrokinetics on deposition mass and rigidity[32]. Silicon dioxide-coated sensors (diameter: 14 mm, AT-cut, roughness < 1 nm, Biolin Scientific, Sweden) were adopted to simulate sand surfaces at nanogram magnitude. The *QCMD* setup comprised an inlet solution reservoir, a *QCMD* chamber with temperature control, a peristaltic pump, and a wastewater container. The peristaltic pump drove a fixed flow velocity of 6×10^{-7} m s^{-1} at static temperatures of 22.5, 25, 27.5, and 30°C, resp.

Before each experiment, a clean sterilized silica sensor was mounted in the chamber, sealed, and connected to the *QCMD* electrodes. Sensor stability and precision were ensured in the air by verifying that both frequency shifts (Δf) and the dissipation shifts (ΔD) remained within ±10% of their standard values across multiple overtones 1, 3, 5, 7, 9, 11, and 13 corresponding to frequencies 5-65 MHz. The baselines were stabilized by pumping ultrapure water for 20 min, followed by 40 min with cell-free PB as a control. For experimental assays, bacterial suspensions in PB were introduced into the *QCMD* system continuously for 2 h with Δf and ΔD monitored simultaneously. Each experiment was performed in duplicate.

Following each *QCMD* experiment, sensors were rinsed with 1.5 mL deionized water in the bottom of a 50 mL centrifuge tube. Subsequently, adhered bacterial cells were detached using

169 an ultrasonic washing unit (FS60, Fisher Scientific, Canada) for 10 min. The sensors were
170 gently transferred to the sensor cater and thoroughly rinsed for two hours with 2% sodium
171 dodecyl sulfate and ultrapure water. After rinsing, the sensors were dried using a nitrogen
172 stream and sterilized for 20 min in a UV chamber for subsequent use. The bacterial cell
173 concentrations in deionized water post-ultrasonic treatment were accurately quantified using a
174 flow cytometer (Novocyte 1040, ACEA, USA), to ensure the data quality for low cell
175 concentrations. Cytometer performance was checked by loading the 1.0 μm diameter blue
176 fluorescent bead standard (FluoSpheres (350/440), lot-no.: F8815, Thermo Fisher Scientific,
177 USA) as the technical calibration before each measurement sequence to ensure the instrument
178 accuracy. Each measurement was conducted in replicates.

179 **2.4 Theory**

180 ***Bacterial collision efficiency in percolation columns*** Although the clean-bed filtration theory
181 refers to an ideal system (i.e., does not encompass heterogeneities in surface charge[33], surface
182 roughness[34], hydration effects, or hydrophobic interaction[35]), it has been found to be a good
183 predictor of bacterial deposition in solutions of high ionic strength (I =0.1−0.3 M)[36,37].

184 For the calculations, we assumed spheres of identical-sized sand particles (average diameter:
185 0.1 mm) in their closest packing and identical effective bacterial radius (1 μm) of the bacteria.
186 The bacterial collision efficiency α_t is used to quantify bacterial deposition and transport
187 according to the clean-bed filtration theory[38]. It can be quantified according to the unit collector
188 efficiency η_t and the transport of particles from bulk solution to the collector surface η_{trans}.

189 The η_{trans} can be quantified by the contributions of convection, diffusion, van der Waals
190 attraction, and sedimentation[24], according to eqs. S1-S3.

191 The η_t can be quantified by fitting the data of influent and effluent cell densities obtained from
192 column experiments, according to eq. 1.[39]

193 $$C = C_0 \exp\left(\frac{3(1-\varepsilon)}{4a_s}\eta_t L\right) \quad (1)$$

194 where C is the effluent cell density, C_0 is the influent cell density, ε is the porosity of the packed
195 porous media, a_s is the radius of the sand particles, L is the length of the column.

196 The collision efficiency α_t is calculated by η_t and η_{trans}, according to eq. 2.[35]

197 $$\alpha_t = \frac{\eta_t}{\eta_{trans}} \quad (2)$$

198 ***QCMD Analyses of Bacterial Transport*** *QCMD* is an acoustic method that reflects the amount
199 and viscoelastic properties of an adhering mass by changes in the resonance frequency (Δf) and
200 energy dissipation (ΔD) of an oscillating crystal-coated sensor surface.[40–42] The shift in
201 resonance frequency, Δf, can be described by the Sauerbrey equation (eq. S6).[43] The $\Delta f/\Delta D$
202 ratio indicates changes in energy dissipation per coupled unit mass and indicates the rigidity
203 and attachment strength of bacterial adhesion.[44–46] Typically, bacterial adhesion leads to a
204 reduction in frequency and an increment in dissipation. Thus, a less negative $\Delta f/\Delta D$ value
205 indicates the buildup of a dissipative soft and fluid film on the *QCMD* sensor. In contrast, more
206 negative values of $\Delta f/\Delta D$ indicate a more rigid layer.

207 ***Quantification of Electrokinetic Forces*** Electroosmosis and electrophoresis are the key
208 electrokinetics driving bacterial transport through porous media, which are related to the zeta
209 potential of porous media and bacteria, respectively. Both of their velocities are related to the
210 liquid viscosity and dielectric constant, the detailed calculations are described in Section S3 in
211 the Supporting Information.

212 # 3. Results and Discussion

213 ## 3.1 Thermal Enhanced Bacterial Transport through Porous Media

214 Bacterial transport was quantified by the breakthrough curves depicted by the normalized
215 effluent cell density (C/C_0) over time represented by pore volume (PV) under temperatures T

= 20-50˚C and electric field strengths E = 0-3 V cm^{-1}, resp. (Fig. 1). The external DC field induced current was 15 mA under 1 V cm^{-1}, producing 0.1˚C temperature increment of water (cf. Section S6 in supporting information), which is hence neglectable in the following discussion. C/C_0 exhibited two stages over time, at the initial stage (the first 2 PV) C/C_0 increased sharply, while in the final stage (last 2 PV), C/C_0 was quasi-steady. Due to the significance of final stage in practical bacterial transport, the average C/C_0 at the final stage was adopted to compare the effects.

At higher temperatures, an increase in C/C_0 was observed, indicating reduced bacterial deposition (Figs. 1A, C, and E). With the absence of electrokinetics, heating from 20 to 50°C increased C/C_0 from 0.16 to 0.72 (ca. 348%). With the presence of 1, 2, and 3 V cm^{-1} electrokinetics, heating increased C/C_0 by 275%, 222%, and 150%, resp. In summary, thermal effects enhanced electrokinetic bacterial transport by $\geqslant$1.5 folds, and the enhancement decreased with increasing DC field strength.

At 20˚C, electrokinetics increased C/C_0 by 0.15 (0.16 to 0.33, at 3 h) (Fig. 1A), and by 0.08, 0.13, 0.13, at 30-50˚C (Figs. 1B-D), resp. This indicated reduced bacterial retention and enhanced transport. Electrokinetic enhancement of *P.* LP6a transport was observed across all temperatures, this enhancement increased with rising DC field strengths and decreased with rising temperatures.

It is notable that temperature increment from 20-30˚C, and 30-40˚C, heating significantly enhanced bacterial transport, C/C_0 increased from 0.16 to 0.46, and from 0.46 to 0.71, resp. at No DC). While from 40-50˚C, C/C_0 was barely increased (0.71-0.72). That is, thermal enhancement has achieved 54.5% efficiency at 30˚C, and the highest efficiency at 40˚C. Meanwhile, flow cytometry viability experiments showed that at 50˚C, 53.79% of bacterial cells were PI stained, compared to 4.35-12.64% at 20-40˚C (Fig. S2). The bacterial viability

has been significantly reduced from 40 to 50˚C. In the context of long-term field application, the temperature range between the soil environment and 30˚C is conducive to the survival and activity of bacterial cells and thus holds more practical significance. Furthermore, the trade-off between the target transport rate and heating consumption within this specific temperature range demands further in-depth investigation.

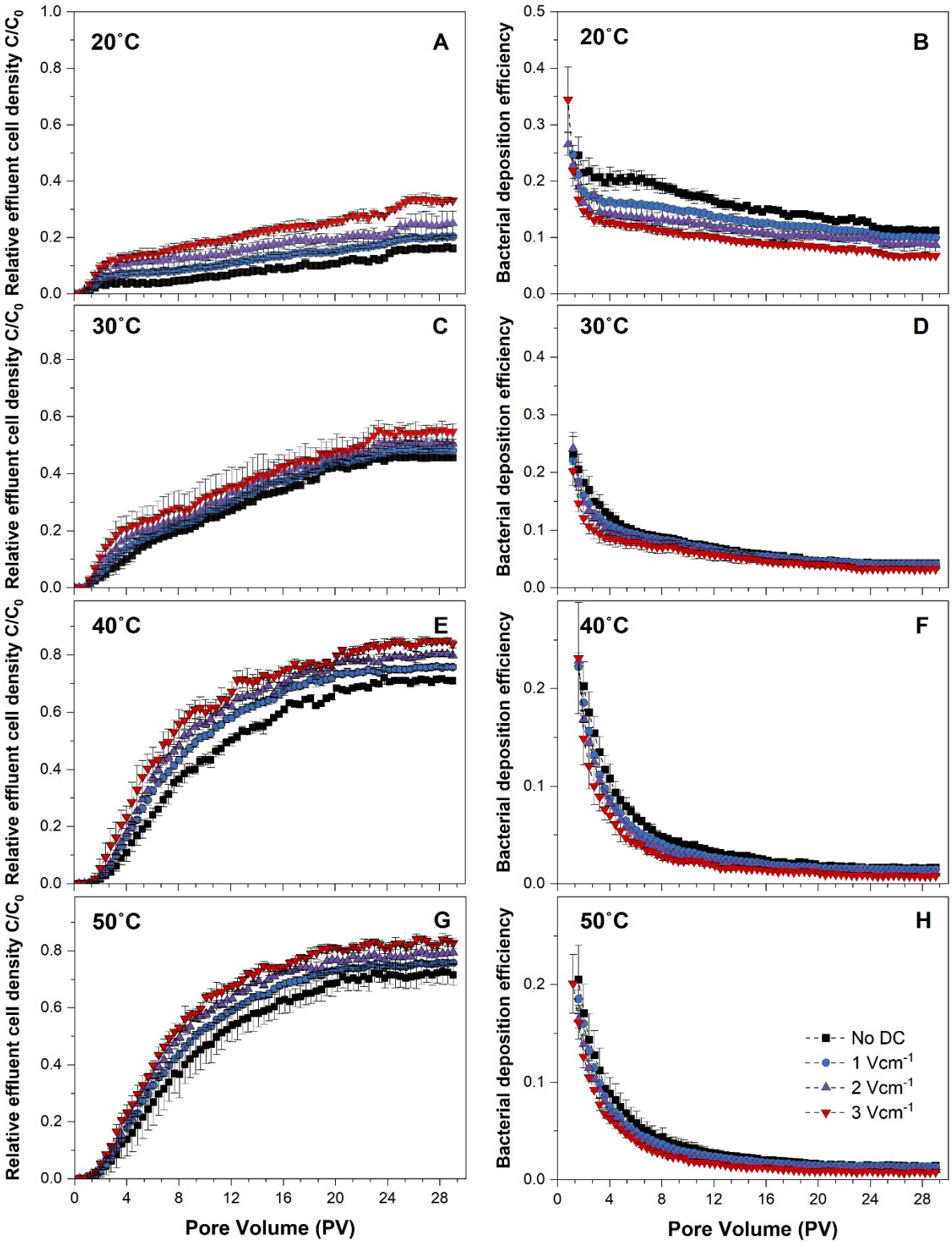

Figure 1. *The relative effluent cell density (A, C, E & G) and collision efficiency (B, D, F & H) of P. LP6a at T=20 (A&B), 30 (C&D), 40 (E&F), and 50˚C (G&H), under electric field strength E = 0 (black), 1 (blue), 2 (purple), and 3 V cm^{-1} (red), resp.*

Based on the breakthrough curves, bacterial collision efficiency in porous media was evaluated using eqs. 1-2 (Figs. 1B, D, F&H). Deposition efficiency at the final stage (α_t) was quantified from the average of the collision efficiency across 10 data points at the plateau (Table 1, Figs. 1&S3).

With temperature increment, both α_t and η_t decreased, while η_{trans} increased, indicating that factor i) η_t was the driving factor in the collision efficiency variations under thermal effects. With heating from 20-50˚C, η_{trans} increased from 1.9% to 2.7%. η_t and bacterial coverage on the sand surface decreased with temperature and DC field strength increment (Fig. S4). Increasing DC fields from 0-2 V cm^{-1} decreased α_t from 5.4 to 3.3 at 20˚C, while thermal effects of 20-40˚C decreased α_t from 5.4 to 1.0. Electrokinetics and heating lead to collision efficiency reduction of 38.9% and 81.5%, resp. That is, a temperature increment of 20˚C leads to 42.6% higher enhancement than the electrokinetic (Fig. S4, Table 1).

Table 1. *Thermal electrokinetic effects on liquid viscosity, electroosmotic flow velocity (v_{EOF}), electrophoretic velocity (v_{EP}), hydraulic flow velocity (v_{HF}), the net velocity (v_{net}) at the secondary minimum distance of DLVO, and the derived bacterial collision efficiency (α_t).*

X (V cm^{-1})	T (°C)	viscosity (mPa s)	dielectric constant	v_{EOF} (10^{-7} m s^{-1})	v_{EP} (10^{-7} m s^{-1})	F_{EOF} (pN)	F_{EP} (pN)	F_{DLVO} (pN)	F_{HF} (pN)	F_{net} (pN)	α_t (×10^{-2})
0	20	1	80.4	0.0	0.0	0.0	0.0	1.2	0.2	1.4	5.4
	30	0.8	76.8	0.0	0.0	0.0	0.0	1.3	0.2	1.5	2.3
	40	0.7	73.3	0.0	0.0	0.0	0.0	1.4	0.2	1.6	1.0
	50	0.6	69.9	0.0	0.0	0.0	0.0	1.5	0.2	2.7	1.0
1	20	1	80.4	5.1	-27.4	1.4	-4.6	1.2	0.2	0.3	4.8
	30	0.8	76.8	6.3	-34.3	1.8	-5.7	1.3	0.2	0.6	2.2
	40	0.7	73.3	7.8	-42.2	2.2	-7.1	1.4	0.2	0.7	0.9
	50	0.6	69.9	9.2	-49.9	2.6	-8.3	1.5	0.2	1.0	0.8
2	20	1	80.4	10.1	-54.9	2.9	-9.2	1.2	0.2	-4.9	4.2
	30	0.8	76.8	12.7	-68.6	3.6	-11.5	1.3	0.2	-6.3	2.0
	40	0.7	73.3	15.6	-84.4	4.4	-14.1	1.4	0.2	-8.1	0.7
	50	0.6	69.9	18.4	-99.8	5.2	-16.7	1.5	0.2	-9.8	0.7
3	20	1	80.4	15.2	-82.3	4.3	-13.8	1.2	0.2	-8.0	3.3
	30	0.8	76.8	19.0	-102.9	5.4	-17.2	1.3	0.2	-10.3	1.8
	40	0.7	73.3	23.4	-126.6	6.6	-21.2	1.4	0.2	-12.9	0.5
	50	0.6	69.9	27.6	-149.7	7.8	-25.0	1.5	0.2	-15.5	0.5

3.2 Correlation of thermal-dependent net force and collision efficiency

Thermal effects on the physicochemical parameters

According to eqs. S7-S10, parameters including i) liquid viscosity η, ii) dielectric constant ε_r, iii) the zeta potentials of bacteria (ζ_b) and solid surface (ζ_s) are key to the DLVO attraction and electrokinetics[23]. As an important environmental parameter, heating from 20°C to 50°C decreases the water viscosity η from 1.00 to 0.55 mPa S, and water dielectric constant ε_r from 80.36 to 69.94.[20,21] The zeta potentials become more negative in higher temperatures following the Smoluchowski equation[22].

Thermal-effect modification on the net force

To further explore the driving mechanisms behind the observed thermal effects on electrokinetic transport, we focused on the quantitative relationship between the net force on the bacterium and its effects on α_t. The net force acting on bacterial cells was quantified by integrating the matrix attraction and electrokinetic forces. The matrix attraction was quantified adopting Derjaguin-Landau-Verwey-Overbeek (DLVO) theory. The DLVO energy (G_{DLVO}) between the bacterium and sand surface at different temperatures was depicted with van der Waals attractive energy and electrostatic repulsive energy, based on measured zeta potential and contact angle properties (Table S1). The attractive energy at the secondary minimal distance (Fig. S5) represents the maximal attractive energy of reversible adhesion. Therefore, the DLVO force (F_{DLVO}) and its interaction with electrokinetic forces were all calculated at the secondary minimal distance.

The net force acting on bacterium (F_{net}) was quantified according to

$$F_{net}(T) = F_{\mathrm{DLVO}}(T) + F_{\mathrm{EOF}}(T) + F_{\mathrm{EP}}(T) + F_{\mathrm{HF}}(T) \quad (3)$$

The detailed equation was deduced to eq. S20, by integrating the DLVO force F_{DLVO}, electroosmotic shear force F_{EOF}, electrophoretic force F_{EP}, and hydraulic shear force F_{HF}, according to eqs. S12-S19.

Electroosmotic flow shear force (F_{EOF}) and electrophoretic force (F_{EP}) were quantified according to eqs. S18-S19. The forces are enhanced by the liquid viscosity and dielectric constant decrement (Fig. 2B, Table 1). At 2 V cm^{-1}, heating increased v_{EOF} from 19.9 to 36.2×10^{-7} m s^{-1}, and increased v_{EP} from -33.3 to -60.6×10^{-7} m s^{-1}, with the '-' sign indicating opposite directions of v_{EOF} and v_{EP}. Heating increased DLVO attractive energy from 5.85×10^{-21} J to 6.4×10^{-21} J (Fig. S5), increased F_{EOF} from 0.8 to 1.6 pN per V cm^{-1}, and F_{EP} from -2.17 to -6.0 pN per V cm^{-1} (Table 1).

The quantified variables were normalized by the data at the temperature of 20˚C to describe their variations. Increasing temperature reduces η linerally to 96% from 20 to 30˚C, while reducing ε_r to 80%. Zeta potentials of bacterium and sand are more negative (i.e., more charged) of up to 79% and 76% (Fig. 2A), which may increase the velocities and forces of electroosmotic flow and electrophoresis.

The variations of the physical environment (i.e, 'direct variables') hence may vary the profiles of DLVO (Fig. S5), and the 'indirect variables' G_{DLVO}, h_s, F_{DLVO}, and F_{net}, further controlling bacterial collision efficiency[48]. F_{net} reflects the net force acting on a bacterium located at the secondary minimal distance, which determines the bacterial collision efficiency, it has a significant variation (up to 20%) and a similar trend as the F_{DLVO}. Meanwhile, heating elevates the kinetic energy of bacterial cells E_{kin} following the Maxwell-Boltzmann distribution[49–51]. The mean value of E_{kin} varied up to 2% (Fig. 2B). From 20-50℃, the mean E_{kin} increased from 6.07×10^{-21} J to 6.69×10^{-2} J. Therefore, 'direct variables' ζ_b, ζ_s, and η, significantly contribute to the variation of 'indirect variables' F_{DLVO} and F_{net} to drive the bacterial collision efficiency.

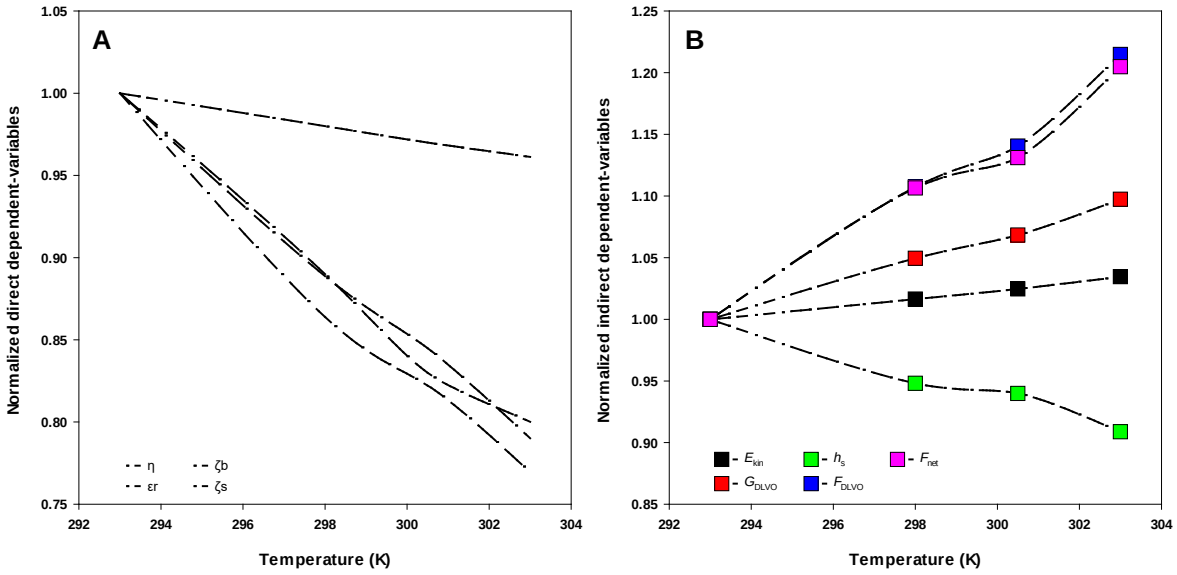

Figure 2. *Temperature effects on the direct (A) and indirect (B) dependent variables determining bacterial collision efficiency.*

The variations of these direct and indirect dependent variables showed that the thermal effects on electrokinetic bacterial transport are more likely determined by the variations in the DLVO interaction energy than that of kinetic energy.

Net force correlation to collision efficiency

Following the previously established framework[28] that interlinked deposition efficiencies (which has included the effects on η_t and η_{trans}) with the net forces (F_{net}) combining the hydraulic flow, electroosmosis, and electrophoresis, we here compared the thermal effects on the F_{net}-α_t correlations at the final stage (Fig. S6).

Under temperatures 20-40˚C, the F_{net} at E = 0, 1, 2 V cm^{-1}, and 3 V cm^{-1} was found to be linearly correlated to the collision efficiency α_t with all $R^2 \geq 0.97$ (Fig. S6), which confirmed the F_{net}-α_t framework in our previous work[28]. While at 50˚C, the R^2 =0.87, indicating weaker linear correlation. This may originate from the 53.79% high cell death at 50˚C. The slopes stand for the rate of F_{net} effects on the collision efficiency (collision efficiency variation per unit net force in *pN*), it decreased from -0.20 to -0.03 with temperature increment from 20-40˚C (Fig.

S6), indicating that temperature has a significant effect on electrokinetic regulated bacterial deposition.

3.3 QCMD Validation of Thermal Effect Mechanisms

QCMD experiments recorded frequency shifts and dissipation shifts at overtones 1, 3, 5, 7, 9, 11, and 13 throughout the 120-min bacterial deposition at 20-30˚C. Overtones are the higher-order resonant frequencies that are integer multiples of the fundamental resonant frequency of the quartz crystal. Frequency shift at overtones reveals mass loading changes on the crystal surface and dissipation shift gives insights into energy-dissipating mechanisms within the adsorbed layer, helping characterize its mechanical properties. The signals showed similar trends in the overtones. Overtone 1 was poorly stable and excessively sensitive, all the other overtones showed relatively stable and similar trends (Fig. S7). Subsequently, we focus our analysis on overtone 5 as the representative signal, using the reference of frequency and dissipation baselines of cell-free PB to calculate the frequency and dissipation shifts.

Figure 2A illustrates Δf_5 and ΔD_5 shifts across temperatures of 20-30˚C and electric field strengths from 0-2 V cm^{-1} of our previous research[32]. Here, pumping bacteria over the sensor surface resulted in a reduction in frequency and an increase in dissipation; Δf_5 and ΔD_5 varied under different experimental conditions (Fig. 3). The shifts of Δf_5 and ΔD_5, exhibited a linear correlation achieving coefficients of determination $R^2 > 0.95$. Therefore, the $\Delta f_5/\Delta D_5$ ratio as an indicator of adhesion rigidity was derived from the slope values (Fig. 3A). Fig. 3B summarizes Δf_5, ΔD_5, and $\Delta f_5/\Delta D_5$ ratios at temperatures 20-30 ˚C. Thermal effects from 20 to 30˚C increased Δf_5 from -27.8 Hz to -11.5 Hz while ΔD_5 increased from 2.4 ppm to 4.8 ppm (Fig. 3B). These shifts led to a reduction in the $\Delta f_5/\Delta D_5$ from -11.6 to -2.4 (i.e., adhesion rigidity reduced 79.3%). On the other hand, with the increment of electric field strengths from 0-2 V cm^{-1}, Δf_5, ΔD_5, and $\Delta f_5/\Delta D_5$ ratios increased (Fig. S8). Δf_5 increased from -12.4 Hz to -3.14 Hz, indicating a 74.7% reduction of bacterial deposition. ΔD_5 increased from 1.89 ppm to 2.34 ppm

indicating a 23.8% less rigid adhesion. The variations of Δf_5 and ΔD_5 resulted in an increment of $\Delta f_5/\Delta D_5$ from -6.56 to -1.34 MHz, that is, the adhesion rigidity was reduced by 79.6%.

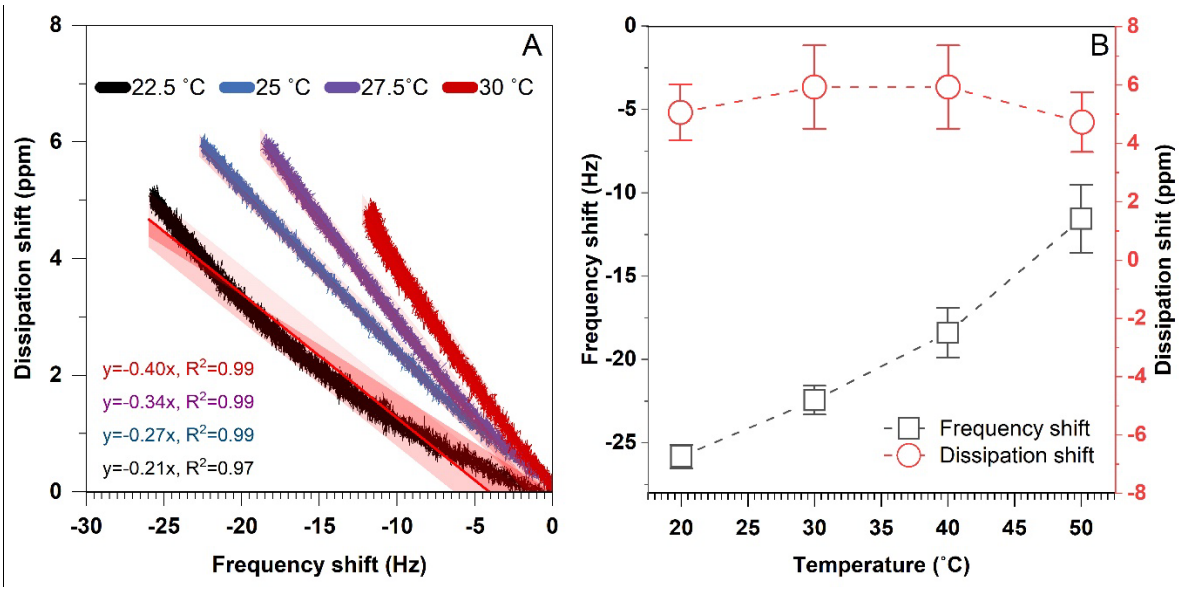

Figure 3. *Thermal (A) and electrokinetic (B) effects on the frequency and dissipation shifts regarding bacterial deposition in the QCMD system, equations and R^2 present the fitting results under temperatures of 22.5˚C (black), 25˚C (blue), 27.5˚C (purple), and 30˚C (red).*

3.4 Primary Contributors of Thermal Effects to the Net Force

Overlaying our previous research on the effects of electric field strength and electrolyte concentration on electrokinetic bacterial transport, the correlations were analyzed with a matrix heatmap (Fig. 4).

The effects of electric field strength and electrophoretic force (F_{EP}) with a relatively high correlation of 0.44 and 0.40, resp. This indicates that the contribution of per unit (V cm^{-1}) electric field is rather higher than per unit temperature (˚C), and the electrokinetic force plays a crucial role in bacterial transport. Electrolyte concentration has dominant effects on the zeta potentials (ζ_b and ζ_s) and double layer thickness κ^{-1}, with correlations > 0.96, temperature has dominant effects on the dielectric constant ε_r, liquid viscosity η, cell kinetic energy E_{kin}, with correlations reach 1.00. This indicates that temperature determines bacterial adhesion rigidity ($\Delta f_5/\Delta D_5$) mainly via dielectric constant ε_r, liquid viscosity η. Temperature varied the primary

contributors dielectric constant ε_r and liquid viscosity η, driving the variations of electrokinetic forces F_{EOF} and F_{EP}, hence determining the adhesion rigidity and transport rate.

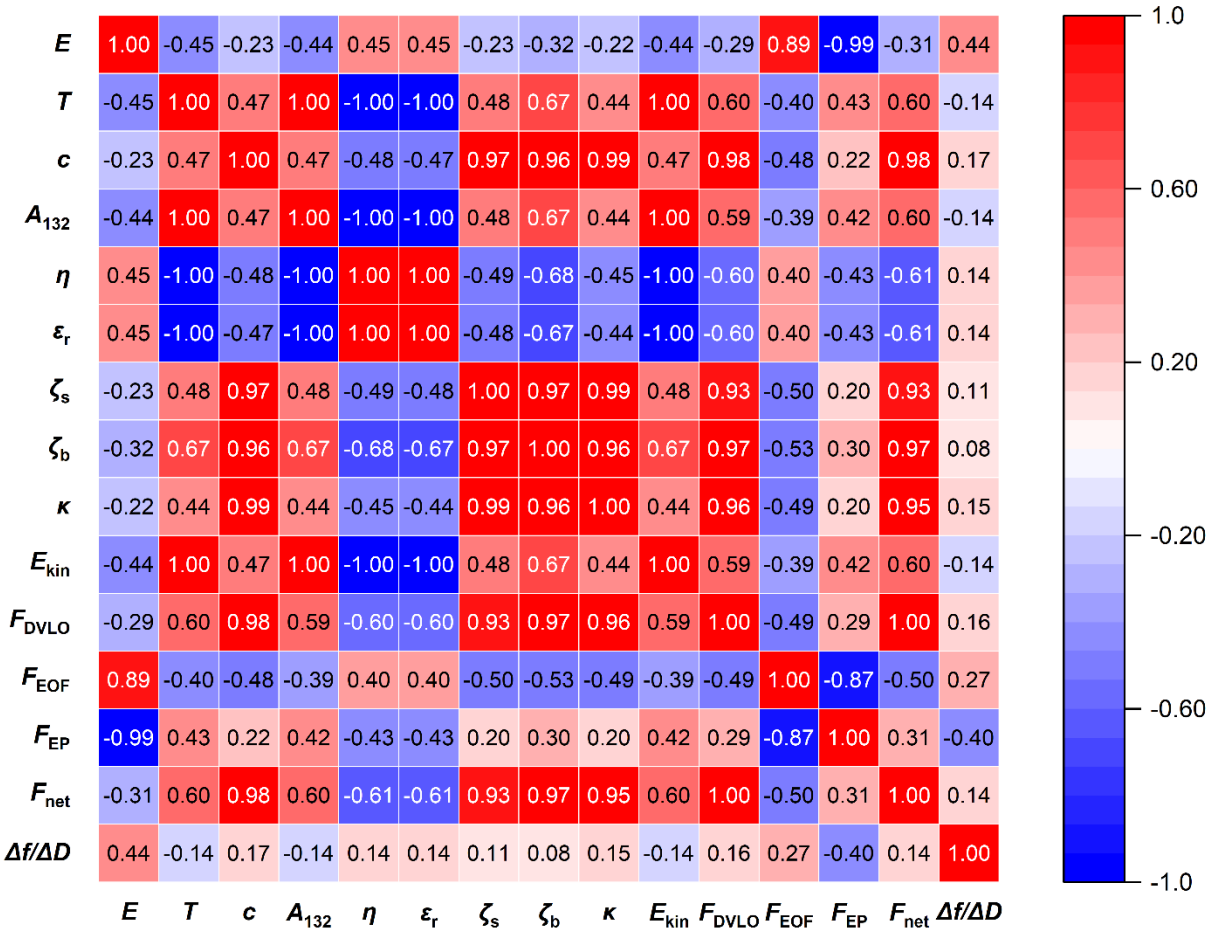

Figure 4. *Correlation between electric field strength (E), temperature (T), buffer concentration (c), intermediate physiochemical properties, and bacterial adhesion rigidity*, red colors represent the extent of positive correlations, while blue colors represent the extent of negative correlations.

3.5 Prediction of Thermal Enhanced Electrokinetic Bacterial Transport

Column transport experiments and *QCMD* characterization revealed the mechanisms of the thermal enhancement of bacterial transport. In practical applications, the quick prediction of the bacterial transport rate is crucial for the engineering design. Based on previous theory analysis, two approaches interlinking DC field strength-temperature-transport enhancement (Fig. 5A), and net force-temperature-transport enhancement (Fig. 5B) were established for

prediction. The warm colors indicate lower collision efficiency, i.e., stronger enhancement of bacterial mobilization, while cold colors indicate higher collision efficiency and weaker enhancement of transport. For porous media with similar physical environment to the experimental system, such as sandy soil, a quick estimation of thermal electrokinetic transport may be achieved with the approach of Fig. 5A. Adapting these approaches in a practical physical environment, measuring the hydrophobicity and zeta potential properties allows the calculation of the net force and prediction of thermal electrokinetic transport in an ideal system. Based on the screened primary contributors of net force, the characterization of physical parameters dielectric constant ε_r and liquid viscosity η, and their variations according to thermal effects may allow for a quick estimation of bacterial transport.

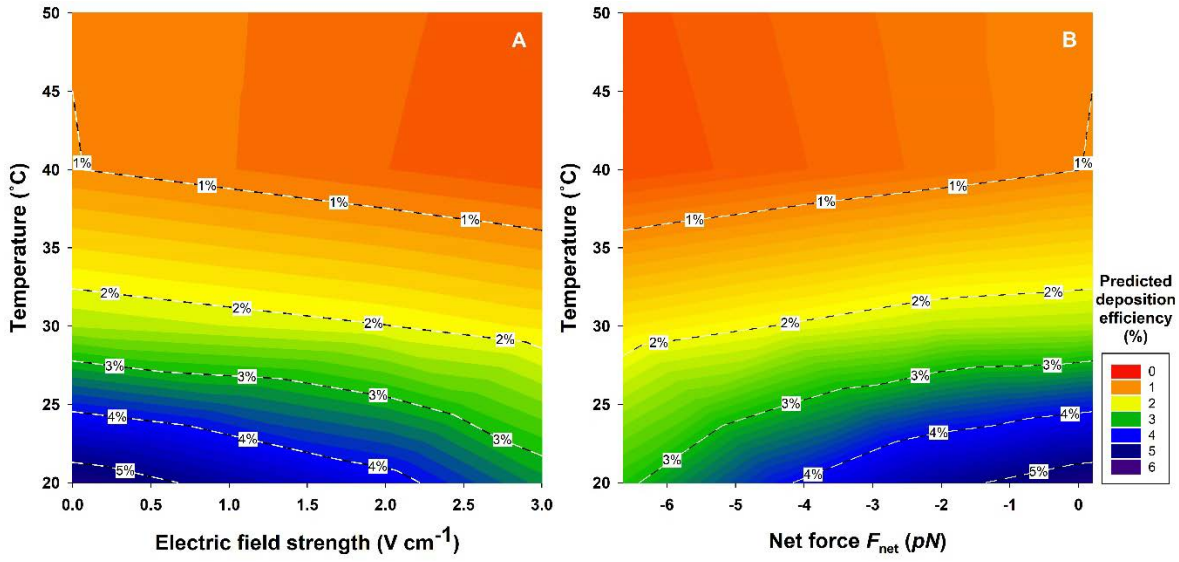

Figure 5. *Temperature-electric field strength (A) and temperature-net force (F_{net}) effects (B) on bacterial collision efficiency, the cold colors indicate higher collision efficiency, while warm colors indicate lower collision efficiency, with data labeled on the boundaries.*

4. Environmental Implications

In this work, the thermal enhancement on electrokinetic bacterial transport has been investigated. The thermal-dependent net force driving mechanisms on electrokinetic bacterial transport have been illustrated. Thermal variations in physical environmental parameters liquid

viscosity, and dielectric constant were the primary contributors of net force shift. An approach interlinking electric field-temperature-efficiency has been established to predict bacterial transport. These findings have been verified by the adhesion behavior in the *QCMD* system at the microscale.

Based on these principles, the thermal electrokinetic approach may be optimized to enhance bacterial transport in the applications of natural and manmade ecosystems. Thermal electrokinetic approaches enhance the transport of functional bacteria to targeted zones in critical processes more efficiently, e.g., facilitating bacterial colonization, fertilization, etc.[52] Based on the screened primary parameters liquid viscosity, and dielectric constant, the net force can be quickly quantified to predict the transport efficiency. In addition, adopting thermophilic bacterial strains[53] in processes e.g., heating desorption soil remediation, allows deriving additional benefits at temperatures up to 60˚C. Knowledge of thermally enhanced electrokinetic effects also allows for improving the management of electrokinetic bacterial dispersal in subsurface porous media e.g. to manipulate microbial community structures and functions in disturbed ecosystems.[54,55]

Together with the previous findings on the thermal electrokinetic transport of chemicals[56,57], the approach may selectively improve specific functions of ecosystems. Besides delivering functional bacterial strains to the target contaminated site, thermal electrokinetic transport also facilitates their accessibility to nutrients facilitating colonization.[58,59] In practice, by adjusting the locations of electrodes and controlling the environmental physiochemical properties, the functional strains may be designed to be located on specified colonizing sites. It should be noted that in practical applications, environmental parameters and technical stability significantly influence bacterial transport. For instance, the tolerance of the applied bio-degrader to DC fields and heating, environmental parameters such as the soil composition

(humic acids, metal nanoparticles, ferric oxide, etc.)[60,61], technical fluctuations, etc. should be investigated. In addition, a comprehensive analysis of the simultaneous transport of nutrients and competing bacteria, which potentially affect the survival of bio-degraders, should be investigated. With overall consideration of the calculated energy consumption of heating and external DC fields (cf. Section S6), and the predicted thermal and electrokinetic effects, the design of temperature adjusting may be optimized to achieve the transport target in practical application. This approach provides new prospects for improving specific functions of ecosystems.

Supporting Information

Theories of bacterial transport, matrix attraction and electrokinetics; Schematic of electrokinetic percolation column reactor; Percentage of PI stained cells of flow cytometry; Thermal electrokinetic effects on bacterial collision efficiency at the final stage; Thermal electrokinetic effects on bacterial coverage, deposition rate, and blocking factor; Profiles of matrix-bacterium interaction and electrokinetics; Frequency and dissipation variations of *QCMD* system; Electrokinetic effects on QCMD bacterial deposition.

Acknowledgments

The authors would like to thank the financial support of the Natural Science Foundation of China (Grant No. 42277011 & 42077126).

References

(1) Tao, X.; Yang, Z.; Feng, J.; Jian, S.; Yang, Y.; Bates, C. T.; Wang, G.; Guo, X.; Ning, D.; Kempher, M. L.; Liu, X. J. A.; Ouyang, Y.; Han, S.; Wu, L.; Zeng, Y.; Kuang, J.; Zhang, Y.; Zhou, X.; Shi, Z.; Qin, W.; Wang, J.; Firestone, M. K.; Tiedje, J. M.; Zhou, J. Experimental Warming Accelerates Positive Soil Priming in a Temperate Grassland Ecosystem. *Nat. Commun.* **2024**, *15* (1), 1178. https://doi.org/10.1038/s41467-024-45277-0.

(2) Stone, B. W.; Li, J.; Koch, B. J.; Blazewicz, S. J.; Dijkstra, P.; Hayer, M.; Hofmockel, K. S.; Liu, X.-J. A.; Mau, R. L.; Morrissey, E. M.; Pett-Ridge, J.; Schwartz, E.; Hungate, B. A. Nutrients Cause Consolidation of Soil Carbon Flux to Small Proportion of Bacterial Community. *Nat. Commun.* **2021**, *12* (1), 3381. https://doi.org/10.1038/s41467-021-23676-x.

(3) Fierer, N. Embracing the Unknown: Disentangling the Complexities of the Soil Microbiome. *Nat. Rev. Microbiol.* **2017**, *15* (10), 579–590. https://doi.org/10.1038/nrmicro.2017.87.

(4) Ruan, Z.; Chen, K.; Cao, W.; Meng, L.; Yang, B.; Xu, M.; Xing, Y.; Li, P.; Freilich, S.; Chen, C.; Gao, Y.; Jiang, J.; Xu, X. Engineering Natural Microbiomes toward Enhanced Bioremediation by Microbiome Modeling. *Nat. Commun.* **2024**, *15* (1), 4694. https://doi.org/10.1038/s41467-024-49098-z.

(5) Cohen, Y.; Pasternak, Z.; Müller, S.; Hübschmann, T.; Schattenberg, F.; Sivakala, K. K.; Abed-Rabbo, A.; Chatzinotas, A.; Jurkevitch, E. Community and Single Cell Analyses Reveal Complex Predatory Interactions between Bacteria in High Diversity Systems. *Nat. Commun.* **2021**, *12* (1), 5481. https://doi.org/10.1038/s41467-021-25824-9.

(6) Scheidweiler, D.; Bordoloi, A. D.; Jiao, W.; Sentchilo, V.; Bollani, M.; Chhun, A.; Engel, P.; De Anna, P. Spatial Structure, Chemotaxis and Quorum Sensing Shape Bacterial Biomass Accumulation in Complex Porous Media. *Nat. Commun.* **2024**, *15* (1), 191. https://doi.org/10.1038/s41467-023-44267-y.

(7) Banerjee, S.; Van Der Heijden, M. G. A. Soil Microbiomes and One Health. *Nat. Rev. Microbiol.* **2023**, *21* (1), 6–20. https://doi.org/10.1038/s41579-022-00779-w.

(8) Livingston, G.; Matias, M.; Calcagno, V.; Barbera, C.; Combe, M.; Leibold, M. A.; Mouquet, N. Competition–Colonization Dynamics in Experimental Bacterial Metacommunities. *Nat. Commun.* **2012**, *3* (1), 1234. https://doi.org/10.1038/ncomms2239.

(9) Wu, L.; Wang, X.-W.; Tao, Z.; Wang, T.; Zuo, W.; Zeng, Y.; Liu, Y.-Y.; Dai, L. Data-Driven Prediction of Colonization Outcomes for Complex Microbial Communities. *Nat. Commun.* **2024**, *15* (1), 2406. https://doi.org/10.1038/s41467-024-46766-y.

(10) Zhu, Y.-G.; Gillings, M.; Simonet, P.; Stekel, D.; Banwart, S.; Penuelas, J. Microbial Mass Movements. *Science* **2017**, *357* (6356), 1099–1100. https://doi.org/10.1126/science.aao3007.

(11) Douterelo, I.; Sharpe, R. L.; Boxall, J. B. Influence of Hydraulic Regimes on Bacterial Community Structure and Composition in an Experimental Drinking Water Distribution System. *Water Res.* **2013**, *47* (2), 503–516. https://doi.org/10.1016/j.watres.2012.09.053.

(12) Rusconi, R.; Guasto, J. S.; Stocker, R. Bacterial Transport Suppressed by Fluid Shear. *Nat. Phys.* **2014**, *10* (3), 212–217. https://doi.org/10.1038/nphys2883.

(13) Kunti, G.; Agarwal, T.; Bhattacharya, A.; Maiti, T. K.; Chakraborty, S. On-Chip Concentration and Patterning of Biological Cells Using Interplay of Electrical and Thermal Fields. *Anal. Chem.* **2020**, *92* (1), 838–844. https://doi.org/10.1021/acs.analchem.9b03364.

(14) Wick, L. Y.; Remer, R.; Würz, B.; Reichenbach, J.; Braun, S.; Schäfer, F.; Harms, H. Effect of Fungal Hyphae on the Access of Bacteria to Phenanthrene in Soil. *Environ. Sci. Technol.* **2007**, *41* (2), 500–505. https://doi.org/10.1021/es061407s.

(15) Shi, L.; Müller, S.; Harms, H.; Wick, L. Y. Factors Influencing the Electrokinetic Dispersion of PAH-Degrading Bacteria in a Laboratory Model Aquifer. *Appl. Microbiol. Biotechnol.* **2008**, *80* (3), 507–515. https://doi.org/10.1007/s00253-008-1577-0.

(16) Semple, Kirk. T.; Doick, K. J.; Jones, K. C.; Burauel, P.; Craven, A.; Harms, H. Defining Bioavailability and Bioaccessibility of Contaminated Soil and Sediment Is Complicated. *Environ. Sci. Technol.* **2004**, *38* (12), 228A-231A. https://doi.org/10.1021/es040548w.

(17) He, J.; Castilla-Alcantara, J. C.; Ortega-Calvo, J. J.; Harms, H.; Wick, L. Y. DC Electric Fields Promote Biodegradation of Waterborne Naphthalene in Biofilter Systems. *Environ. Sci. Technol.* **2024**, acs.est.4c02924. https://doi.org/10.1021/acs.est.4c02924.

(18) Shan, Y.; Harms, H.; Wick, L. Y. Electric Field Effects on Bacterial Deposition and Transport in Porous Media. *Environ. Sci. Technol.* **2018**, *52* (24), 14294–14301. https://doi.org/10.1021/acs.est.8b03648.

(19) Qin, J.; Sun, X.; Liu, Y.; Berthold, T.; Harms, H.; Wick, L. Y. Electrokinetic Control of Bacterial Deposition and Transport. *Environ. Sci. Technol.* **2015**, *49* (9), 5663–5671. https://doi.org/10.1021/es506245y.

(20) Podolsky, R. D. Temperature and Water Viscosity: Physiological Versus Mechanical Effects on Suspension Feeding. *Science* **1994**, *265* (5168), 100–103. https://doi.org/10.1126/science.265.5168.100.

(21) Malmberg, C.; Maryott, A. Dielectric Constant of Water from 00 to 1000 C. *J. Res. Natl. Bur. Stand.* **1956**, *56* (1), 1–8.

(22) Constantin, P.; Kevrekidis, I.; S. Titi, E. Remarks on a Smoluchowski Equation. *Discrete Contin. Dyn. Syst.* **2004**, *11* (1), 101–112. https://doi.org/10.3934/dcds.2004.11.101.

(23) *Particle Deposition and Aggregation: Measurement, Modelling and Simulation*; Elimelech, M., Ed.; Colloid and surface engineering series; Butterworth-Heinemann: Oxford, 1998.

(24) Martin, R. E.; Bouwer, E. J.; Hanna, L. M. Application of Clean-Bed Filtration Theory to Bacterial Deposition in Porous Media. *Environ. Sci. Technol.* **1992**, *26* (5), 1053–1058. https://doi.org/10.1021/es00029a028.

(25) Foght, J. M.; Westlake, D. W. Transposon and Spontaneous Deletion Mutants of Plasmid-Borne Genes Encoding Polycyclic Aromatic Hydrocarbon Degradation by a Strain of Pseudomonas Fluorescens. *Biodegradation* **1996**, *7* (4), 353–366.

(26) Ghanem, N.; Kiesel, B.; Kallies, R.; Harms, H.; Chatzinotas, A.; Wick, L. Y. Marine Phages As Tracers: Effects of Size, Morphology, and Physico–Chemical Surface Properties on Transport in a Porous Medium. *Environ. Sci. Technol.* **2016**, *50* (23), 12816–12824. https://doi.org/10.1021/acs.est.6b04236.

(27) Achtenhagen, J.; Goebel, M.-O.; Miltner, A.; Woche, S. K.; Kästner, M. Bacterial Impact on the Wetting Properties of Soil Minerals. *Biogeochemistry* **2015**, *122* (2–3), 269–280. https://doi.org/10.1007/s10533-014-0040-9.

(28) Shan, Y.; Harms, H.; Wick, L. Y. Electric Field Effects on Bacterial Deposition and Transport in Porous Media. *Environ. Sci. Technol.* **2018**, *52* (24), 14294–14301. https://doi.org/10.1021/acs.est.8b03648.

(29) Feiler, A. A.; Sahlholm, A.; Sandberg, T.; Caldwell, K. D. Adsorption and Viscoelastic Properties of Fractionated Mucin (BSM) and Bovine Serum Albumin (BSA) Studied with Quartz Crystal Microbalance (QCM-D). *J. Colloid Interface Sci.* **2007**, *315* (2), 475–481. https://doi.org/10.1016/j.jcis.2007.07.029.

(30) Olsson, A. L. J.; van der Mei, H. C.; Busscher, H. J.; Sharma, P. K. Acoustic Sensing of the Bacterium–Substratum Interface Using QCM-D and the Influence of Extracellular Polymeric Substances. *J. Colloid Interface Sci.* **2011**, *357* (1), 135–138. https://doi.org/10.1016/j.jcis.2011.01.035.

(31) Olsson, A. L. J.; van der Mei, H. C.; Busscher, H. J.; Sharma, P. K. Acoustic Sensing of the Bacterium–Substratum Interface Using QCM-D and the Influence of Extracellular Polymeric Substances. *J. Colloid Interface Sci.* **2011**, *357* (1), 135–138. https://doi.org/10.1016/j.jcis.2011.01.035.

(32) Shan, Y.; Liu, L.; Liu, Y.; Harms, H.; Wick, L. Y. Effects of Electrokinetic Phenomena on Bacterial Deposition Monitored by Quartz Crystal Microbalance with Dissipation Monitoring. *Environ. Sci. Technol.* **2020**, *54* (21), 14036–14045. https://doi.org/10.1021/acs.est.0c04347.

(33) Elimelech, M.; Chen, J. Y.; Kuznar, Z. A. Particle Deposition onto Solid Surfaces with Micropatterned Charge Heterogeneity: The “Hydrodynamic Bump” Effect. *Langmuir* **2003**, *19* (17), 6594–6597. https://doi.org/10.1021/la034516i.

(34) Bhattacharjee, S.; Ko, C.-H.; Elimelech, M. DLVO Interaction between Rough Surfaces. *Langmuir* **1998**, *14* (12), 3365–3375. https://doi.org/10.1021/la971360b.

(35) Elimelech, M. *Particle Deposition and Aggregation: Measurement, Modelling, and Simulation*; Colloid and surface engineering series; Butterworth-Heinemann: Woburn, 1998.

(36) Redman, J. A.; Walker, S. L.; Elimelech, M. Bacterial Adhesion and Transport in Porous Media: Role of the Secondary Energy Minimum. *Environ. Sci. Technol.* **2004**, *38* (6), 1777–1785. https://doi.org/10.1021/es034887l.

(37) Simoni, S. F.; Bosma, T. N. P.; Harms, H.; Zehnder, A. J. B. Bivalent Cations Increase Both the Subpopulation of Adhering Bacteria and Their Adhesion Efficiency in Sand Columns. *Environ. Sci. Technol.* **2000**, *34* (6), 1011–1017. https://doi.org/10.1021/es990476m.

(38) Velasco-Casal, P.; Wick, L. Y.; Ortega-Calvo, J.-J. Chemoeffectors Decrease the Deposition of Chemotactic Bacteria during Transport in Porous Media. *Environ. Sci. Technol.* **2008**, *42* (4), 1131–1137. https://doi.org/10.1021/es071707p.

(39) Ryan, J. N.; Elimelech, M. Colloid Mobilization and Transport in Groundwater. *Colloids Surf. Physicochem. Eng. Asp.* **1996**, *107*, 1–56. https://doi.org/10.1016/0927-7757(95)03384-X.

(40) Ward, M. D.; Buttry, D. A. In Situ Interfacial Mass Detection with Piezoelectric Transducers. *Science* **1990**, *249* (4972), 1000–1007.

(41) Reviakine, I.; Johannsmann, D.; Richter, R. P. Hearing What You Cannot See and Visualizing What You Hear: Interpreting Quartz Crystal Microbalance Data from Solvated Interfaces. *Anal. Chem.* **2011**, *83* (23), 8838–8848. https://doi.org/10.1021/ac201778h.

(42) Camesano, T. A.; Liu, Y.; Datta, M. Measuring Bacterial Adhesion at Environmental Interfaces with Single-Cell and Single-Molecule Techniques. *Adv. Water Resour.* **2007**, *30* (6–7), 1470–1491. https://doi.org/10.1016/j.advwatres.2006.05.023.

(43) Sauerbrey, G. Verwendung von Schwingquarzen zur Wägung dünner Schichten und zur Mikrowägung. *Z. Für Phys.* **1959**, *155* (2), 206–222. https://doi.org/10.1007/BF01337937.

(44) Gutman, J.; Walker, S. L.; Freger, V.; Herzberg, M. Bacterial Attachment and Viscoelasticity: Physicochemical and Motility Effects Analyzed Using Quartz Crystal Microbalance with Dissipation (QCM-D). *Environ. Sci. Technol.* **2013**, *47* (1), 398–404. https://doi.org/10.1021/es303394w.

(45) Kao, W.-L.; Chang, H.-Y.; Lin, K.-Y.; Lee, Y.-W.; Shyue, J.-J. Effect of Surface Potential on the Adhesion Behavior of NIH3T3 Cells Revealed by Quartz Crystal Microbalance with Dissipation Monitoring (QCM-D). *J. Phys. Chem. C* **2017**, *121* (1), 533–541. https://doi.org/10.1021/acs.jpcc.6b11217.

(46) Marcus, I. M.; Herzberg, M.; Walker, S. L.; Freger, V. Pseudomonas Aeruginosa Attachment on QCM-D Sensors: The Role of Cell and Surface Hydrophobicities. *Langmuir* **2012**, *28* (15), 6396–6402. https://doi.org/10.1021/la300333c.

(47) Rijnaarts, H. H. M.; Norde, W.; Bouwer, E. J.; Lyklema, J.; Zehnder, A. J. B. Bacterial Deposition in Porous Media Related to the Clean Bed Collision Efficiency and to Substratum Blocking by Attached Cells. *Environ. Sci. Technol.* **1996**, *30* (10), 2869–2876. https://doi.org/10.1021/es960597b.

(48) Shan, Y.; Harms, H.; Wick, L. Y. Electric Field Effects on Bacterial Deposition and Transport in Porous Media. *Environ. Sci. Technol.* **2018**, *52* (24), 14294–14301. https://doi.org/10.1021/acs.est.8b03648.

(49) Mo, J.; Raizen, M. G. Highly Resolved Brownian Motion in Space and in Time. *Annu. Rev. Fluid Mech.* **2019**, *51* (1), 403–428. https://doi.org/10.1146/annurev-fluid-010518-040527.

(50) Li, G.; Tam, L.-K.; Tang, J. X. Amplified Effect of Brownian Motion in Bacterial Near-Surface Swimming. *Proc. Natl. Acad. Sci.* **2008**, *105* (47), 18355–18359. https://doi.org/10.1073/pnas.0807305105.

(51) Mackay, M. E.; Tuteja, A.; Duxbury, P. M.; Hawker, C. J.; Van Horn, B.; Guan, Z.; Chen, G.; Krishnan, R. S. General Strategies for Nanoparticle Dispersion. *Science* **2006**, *311* (5768), 1740–1743. https://doi.org/10.1126/science.1122225.

(52) Gude, S.; Pinçe, E.; Taute, K. M.; Seinen, A.-B.; Shimizu, T. S.; Tans, S. J. Bacterial Coexistence Driven by Motility and Spatial Competition. *Nature* **2020**, *578* (7796), 588–592. https://doi.org/10.1038/s41586-020-2033-2.

(53) Parameswaran, P.; Bry, T.; Popat, S. C.; Lusk, B. G.; Rittmann, B. E.; Torres, C. I. Kinetic, Electrochemical, and Microscopic Characterization of the Thermophilic, Anode-Respiring Bacterium

Thermincola Ferriacetica. *Environ. Sci. Technol.* **2013**, *47* (9), 4934–4940. https://doi.org/10.1021/es400321c.

(54) König, S.; Worrich, A.; Banitz, T.; Centler, F.; Harms, H.; Kästner, M.; Miltner, A.; Wick, L. Y.; Thullner, M.; Frank, K. Spatiotemporal Disturbance Characteristics Determine Functional Stability and Collapse Risk of Simulated Microbial Ecosystems. *Sci. Rep.* **2018**, *8* (1), 9488.

(55) König, S.; Worrich, A.; Banitz, T.; Harms, H.; Kästner, M.; Miltner, A.; Wick, L. Y.; Frank, K.; Thullner, M.; Centler, F. Functional Resistance to Recurrent Spatially Heterogeneous Disturbances Is Facilitated by Increased Activity of Surviving Bacteria in a Virtual Ecosystem. *Front. Microbiol.* **2018**, *9*, 734.

(56) Qin, J.; Moustafa, A.; Harms, H.; El-Din, M. G.; Wick, L. Y. The Power of Power: Electrokinetic Control of PAH Interactions with Exfoliated Graphite. *J. Hazard. Mater.* **2015**, *288*, 25–33. https://doi.org/10.1016/j.jhazmat.2015.02.008.

(57) Shan, Y.; Hao, H.; Yin, Y.; Hu, N.; Zhan, M.; Ma, D.; Yin, Y.; Jiao, W.; Wick, L. Y. Effects of Temperature and DC Electric Fields on Perfluorooctanoic Acid Sorption Kinetics to Activated Carbon. *Environ. Sci. Technol.* **2024**, *58* (13), 5987–5995. https://doi.org/10.1021/acs.est.3c10590.

(58) Mao, X.; Wang, J.; Ciblak, A.; Cox, E. E.; Riis, C.; Terkelsen, M.; Gent, D. B.; Alshawabkeh, A. N. Electrokinetic-Enhanced Bioaugmentation for Remediation of Chlorinated Solvents Contaminated Clay. *J. Hazard. Mater.* **2012**, *213–214*, 311–317. https://doi.org/10.1016/j.jhazmat.2012.02.001.

(59) Sprocati, R.; Gallo, A.; Sethi, R.; Rolle, M. Electrokinetic Delivery of Reactants: Pore Water Chemistry Controls Transport, Mixing, and Degradation. *Environ. Sci. Technol.* **2021**, *55* (1), 719–729. https://doi.org/10.1021/acs.est.0c06054.

(60) Yang, H.; Ge, Z.; Wu, D.; Tong, M.; Ni, J. Cotransport of Bacteria with Hematite in Porous Media: Effects of Ion Valence and Humic Acid. *Water Res.* **2016**, *88*, 586–594. https://doi.org/10.1016/j.watres.2015.10.052.

(61) Abramson, A.; Brown, D. G. Influence of Solution Ionic Strength on the Collision Efficiency Distribution and Predicted Transport Distance of a Sphingomonas Sp. Flowing through Porous Media. *Water Res.* **2007**, *41* (19), 4435–4445. https://doi.org/10.1016/j.watres.2007.06.005.